

Lighting Model for Underwater Photogrammetric Captures

Nathan Hui¹, Eric Lo¹, Dominique Rissolo¹, Falko Kuester¹

¹ Cultural Heritage Engineering Initiative, University of California San Diego, La Jolla, California, USA
(nthui, eklo, drissolo, fkuester)@ucsd.edu

Keywords: Underwater photogrammetry, lighting model

Abstract

Photogrammetry is an established technique for producing 3D representations of submerged structures in shallow, naturally lit environments. Natural light is not available in more extreme environments such as in the deep ocean or submerged caves, which are major applications for photogrammetric survey. Additionally, these environments are often accessed with resource-limited sensor platforms, necessitating efficient use of power constraining the level of artificial illumination that can be deployed. A method to estimate the amount of light needed to achieve sufficient image quality in underwater photogrammetric acquisition systems is presented.

1. Introduction

Photogrammetry, and particularly underwater photogrammetry, relies heavily on clear and sharp images to enable feature detection and localization (Bobkowska et al., 2021, Burdziakowski and Bobkowska, 2021). Recent developments in underwater photogrammetry applications are increasing the path loss of light in the imagery, whether due to increasing standoff distances, turbid environments, cloud cover, time of day, caustics, etc (Song et al., 2022). With many of these new applications occurring in a limited light environment (such as benthic or overhead environments), motion will typically be a major contributor to image blurriness. Dynamic elements of ocean environments such as surge, swell, and current will contribute to camera motion.

In photography, we can adjust parameters such as shutter speed, aperture, ISO, and illumination to achieve the desired exposure. In underwater photography, many of these parameters are constrained due to the low light environment, thus, bringing additional light allows more flexibility in achieving appropriate image quality. Modeling the required lighting allows us to determine a design's ability to meet mission requirements. Recent research primarily focuses on optimizing the light placement to reduce loss due to backscatter (Song et al., 2021) or color correction (Song and Baik, 2023).

We can eliminate motion blur by limiting the exposure to the time it takes for the camera's projected image to traverse 1 pixel, meaning that, the exposure is constrained such that the maximum blur is 1 pixel. This constraint will drive selection of lens aperture and ISO value. Additional light can also be brought to bear on the scene, which will allow more ideal lens aperture and ISO values. Insufficient light will result in too large an aperture (shallow depth of focus) or too high of an ISO value (increased graininess). Excess light will result in a smaller aperture (larger depth of focus) and lower ISO value (reduced noise), up to practical limits.

To simplify the formulation, we assume the following:

- Scene is planar and normal to the optical axis, and is uniformly reflective.

- Artificial illumination is uniform over the beam width and visible scene.
- Image degradation due to backscatter is not considered.
- Camera is infinitely sharp.
- Camera is moving parallel to the scene and towards the "up" direction of the image.

2. Definition of Terms

We denote source parameters with the subscript Σ .

- θ_{Σ} 1-D angular width of the light source beam in rad
- $\Phi_{v,\Sigma}$ Illumination source luminous power in lm
- z_{Σ} Illumination source altitude over scene in m
- A_{Σ} Planar area of illumination at the scene in m^2
- Ω_{Σ} Illumination source solid angle (2-D angular width) in sr

We denote camera parameters with the subscript c .

- f_c Camera lens focal length in m
- N_c Camera lens aperture size in f-number
- I_c Camera exposure index ("Film Speed") in ISO units
- z_c Imager altitude over the scene in m
- w_c Camera sensor width in m
- h_c Camera sensor height in m
- p_c Camera sensor pixel pitch in m
- v_c Forward velocity of the camera in $m\ s^{-1}$
- Ω_c Camera view solid angle (2-D angular width) in sr
- t_c Exposure time in s

- $L_{v,c}$ Scene luminance as seen by the camera in cd m^{-2}

We denote the projected image parameters with the subscript I .

- w_I Camera projected image width in m
- h_I Camera projected image height in m
- A_I Camera projected image area in m^2

We denote scene parameters with the subscript S .

- r_S Scene reflectivity as a value from 0 to 100 in %
- $E_{v,S}$ Total luminous flux incident on scene in lx
- $M_{v,S}$ Total luminous flux reflected from scene lx
- $L_{v,S}$ Scene luminance in cd m^{-2}

We denote Secchi parameters with the subscript d .

- z_d Secchi distance in m
- k_d Light extinction coefficient

These values are constants provided by ISO 12232:2019 (International Organization for Standardization, 2019).

- H_m Average focal plane exposure¹ in lx s
- q Focal plane exposure correction factor (approx. 0.65 sr^2) in sr
- K Exposure Index reference exposure (10 lx s^3) in lx s

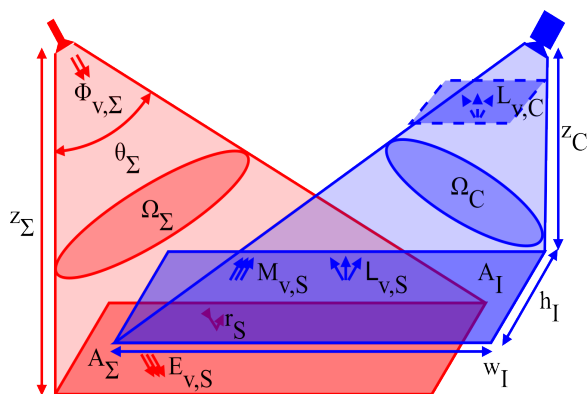


Figure 1. Diagram of terms. Red elements are associated with the artificial illumination source. Blue elements are associated with the reflected light and camera.

¹ See ISO 12232:2019(E) Section 4.1

² See ISO 12232:2019(E) Equation B.2 and B.4

³ See ISO 12232:2019(E) Section 4.1

3. Model Derivation

$$A_{\Sigma} = \pi \left(z_{\Sigma} \tan \left(\frac{\theta_{\Sigma}}{2} \right) \right)^2 \quad (1)$$

$$w_I = \frac{z_c w_c}{f_c} \quad (2)$$

$$h_I = \frac{z_c h_c}{f_c} \quad (3)$$

$$A_I = w_I h_I \quad (4)$$

We first compute the projected areas of both the camera view and the artificial illumination. The illuminated area we compute using Equation 1. The projected camera view area is computed with Equation 4

$$\Omega_{\Sigma} = 2\pi \left(1 - \cos \left(\frac{\theta_{\Sigma}}{2} \right) \right) \quad (5)$$

$$\Omega_c = 4 \arctan \frac{A_I}{2z_c \sqrt{4z_c^2 + w_I^2 + h_I^2}} \quad (6)$$

$$= 4 \arctan \frac{\frac{z_c w_c}{f_c} \frac{z_c h_c}{f_c}}{2z_c \sqrt{4z_c^2 + \left(\frac{z_c w_c}{f_c} \right)^2 + \left(\frac{z_c h_c}{f_c} \right)^2}} \quad (7)$$

$$= 4 \arctan \frac{w_c h_c}{2f_c \sqrt{4f_c^2 + w_c^2 + h_c^2}} \quad (8)$$

We next compute the solid angle Ω_{Σ} in sr using Equation 5. This provides us a measure of the “size” of the illumination beam. We also compute the solid angle Ω_c in sr of the camera view using Equation 6.

$$I_z = I_0 e^{-k_d z} \quad (9)$$

$$k_d = \frac{1.7}{z_d} \quad (10)$$

$$E_{v,S} = \frac{\Phi_{v,\Sigma}}{A_{\Sigma}} e^{-k_d z_{\Sigma}} \quad (11)$$

$$M_{v,S} = E_{v,S} r_S \quad (12)$$

We then need to compute the light attenuation down through the water column. Idso and Gilbert provide a model for this, shown in Equations 9 and 10 (Idso and Gilbert, 1974). We apply these to the illumination sources present in the scene (artificial light and solar), resulting in Equation 11.

Since no scene reflects 100% of light, we account for some loss of light due to scene absorption with scene reflectivity r_S in %. The reflected luminous flux $M_{v,S}$ from the scene is given by Equation 12.

$$L_{v,S} = \frac{M_{v,S}}{\Omega_c} \quad (13)$$

$$L_{v,c} = L_{v,S} e^{-k_d z_c} \quad (14)$$

We assume that the scene is well lit. Thus, the luminance of the scene is given by Equation 13. Since the light traveling from

the scene to the camera is still subject to attenuation, we need to again take into account this path loss. The scene luminance from the camera's perspective is given by Equation 14.

$$H_m = \frac{qL_{v,S}t_c}{N_c^2} \quad (15)$$

$$I_c = \frac{K}{H_m} \quad (16)$$

$$L_{v,c} = \frac{KN_c^2}{qI_c t_c} \quad (17)$$

ISO 12232:2019 provides the math to relate $L_{v,S}$, I_c , and t_c , shown in Equation 15 and Equation 16 (International Organization for Standardization, 2019). We can rearrange these to facilitate computing the scene luminance, shown in Equation 17.

$$L_{v,c} = \frac{KN_c^2}{qI_c t_c} \quad (18)$$

$$L_{v,S} e^{-k_d z_c} = \frac{KN_c^2}{qI_c t_c} \quad (19)$$

$$\frac{M_{v,S}}{\Omega_c} e^{-k_d z_c} = \frac{KN_c^2}{qI_c t_c} \quad (20)$$

$$E_{v,S} r_S e^{-\frac{1.7}{z_d} z_c} = \frac{KN_c^2 \Omega_c}{qI_c t_c} \quad (21)$$

We can then formalize the entire artificial light model with respect to illuminance in Equation 21. We discuss these terms and their significance and semantics in section 4.

4. Model Discussion

We can broadly break up Equation 21 into a few major groups. $E_{v,S}$ is the light from the artificial light source. $\frac{N_c^2 \Omega_c}{I_c t_c}$ are the camera exposure parameters.

We can intuit the left side of Equation 21 as the "amount" of light coming into the camera, and the right side of Equation 21 as the camera parameters required to achieve a nominally exposed image.

The relationship between the aperture size N_c , ISO speed I_c , and exposure time t_c is what we expect from photography. Imaging a brighter scene requires decreasing t_c or I_c , or making the aperture smaller (increasing N_c). Correspondingly, doubling t_c (increasing by one stop) can be compensated by closing the aperture (reducing by one stop) or by halving the ISO speed (decreasing by one stop).

Figure 2 shows an example of the relationship between focal length f_c and the camera solid angle Ω_c , for which the expanded model is given in Equation 8. Over the domain of possible values of f_c , w_c , and h_c , \arctan will have a range of $[0, \frac{\pi}{2})$, and as a result, Ω_c has a range of $[0, 2\pi)$ sr (half of a sphere). An example curve of this behavior is shown in Figure 2. Due to this, f_c , w_c , and h_c have a very limited influence on the exposure behavior of the camera system.

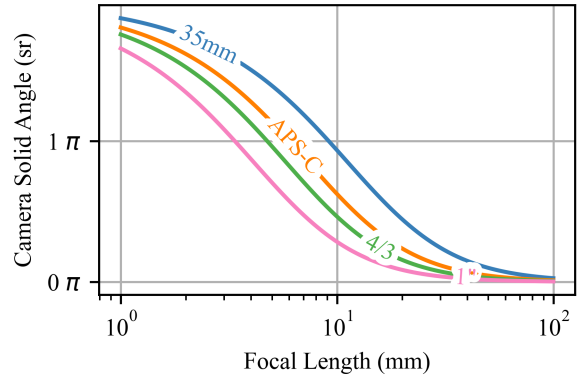


Figure 2. Camera solid angle vs focal length for various sensor sizes

If we expand the illuminance terms, we get the following:

$$E_{v,S} = \frac{\Phi_{v,\Sigma}}{A_\Sigma} e^{-k_S z_\Sigma} \quad (22)$$

$$= \frac{\Phi_{v,\Sigma}}{\pi (z_\Sigma \tan(\frac{\theta_\Sigma}{2}))^2} e^{-k_S z_\Sigma} \quad (23)$$

$$= \frac{\Phi_{v,\Sigma}}{\pi (z_\Sigma \tan(\frac{\theta_\Sigma}{2}))^2} e^{-\frac{1.7 z_\Sigma}{z_d}} \quad (24)$$

If we look at a scenario in which we only have artificial lighting, the model becomes

$$E_{v,S(\Sigma)} r_S e^{-\frac{1.7 z_c}{z_d}} = \frac{K N_c^2 \Omega_c}{q I_c t_c} \quad (25)$$

$$\frac{\Phi_{v,\Sigma}}{A_\Sigma} r_S e^{-k_d z_\Sigma} e^{-\frac{1.7 z_c}{z_d}} = \frac{K N_c^2 \Omega_c}{q I_c t_c} \quad (26)$$

$$\frac{\Phi_{v,\Sigma}}{\pi (z_\Sigma \tan(\frac{\theta_\Sigma}{2}))^2} r_S e^{-\frac{1.7}{z_d} (z_\Sigma + z_c)} = \frac{K N_c^2 \Omega_c}{q I_c t_c} \quad (27)$$

Often, we want to apply this model to see how much light we need for a particular environment. The exposure time t_c is limited by motion blur. This can be computed from the camera velocity v_c in m s^{-1} , pixel pitch p_c in m, focal length f_c in m, and camera altitude z_c in m as shown in Equation 28.

$$t_c \leq \frac{z_c p_c}{f_c v_c} \quad (28)$$

Rearranging the artificial light model (Equation 27) results in Equation 29.

$$t_c = \frac{K N_c^2 \Omega_c}{q I_c} \frac{\pi z_\Sigma^2 \tan^2(\frac{\theta_\Sigma}{2}) e^{\frac{1.7}{z_d} (z_\Sigma + z_c)}}{\Phi_{v,\Sigma} r_S} \quad (29)$$

Since the light from the artificial source is not collimated and experiences appreciable spread over distance, we have a significant dependency on the artificial light source altitude z_Σ in Equation 29. The z_Σ^2 term significantly limits the impact of artificial lighting at significant standoff distances such that it is

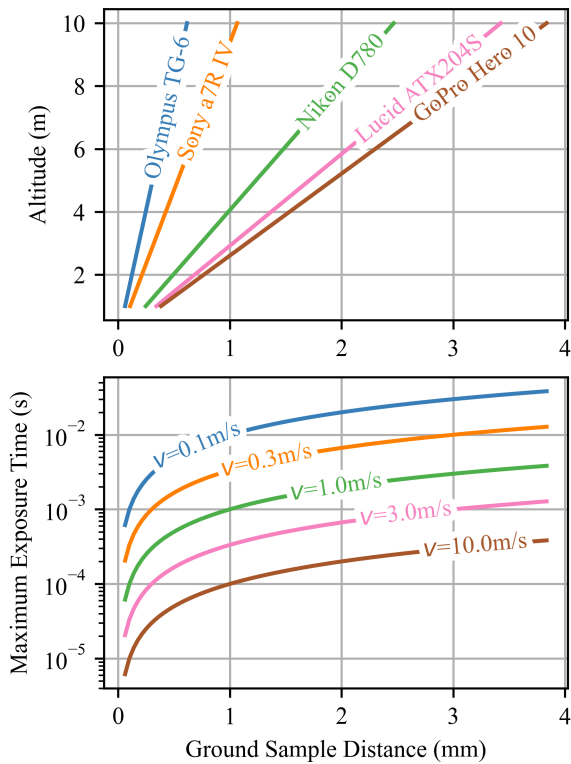


Figure 3. Sample pixel size (Ground Sample Distance) and shutter speed limit curves. Cameras in order are: Olympus TG-6 with 25 mm lens, Sony a7R IV with 35 mm lens, Nikon D780 with 24 mm lens, Lucid ATX204S with 8 mm lens, and GoPro Hero 10

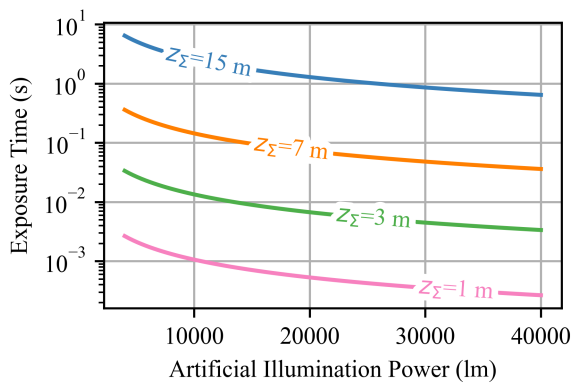


Figure 4. Example exposure time curves for various artificial illumination powers and survey altitudes. $z_d = 20$ m, $z_\Sigma = z_c$, $E_{v,A} = 0$

more effective to be closer to the scene than it is to double the amount the light carried. This is demonstrated in Figure 4.

Looking at this model from the perspective of how much light is required to illuminate a given scene, we get the curves in Figure 5. Current LED technology can achieve on the order of 200 lm W^{-1} to 300 lm W^{-1} . Thus, in order to achieve millisecond exposure times at a range of 10 m with ISO 1600, we need to generate on the order of 1×10^6 lm, requiring approximately 4 kW, which would be about enough to boil a liter of 5°C water in 2 min.

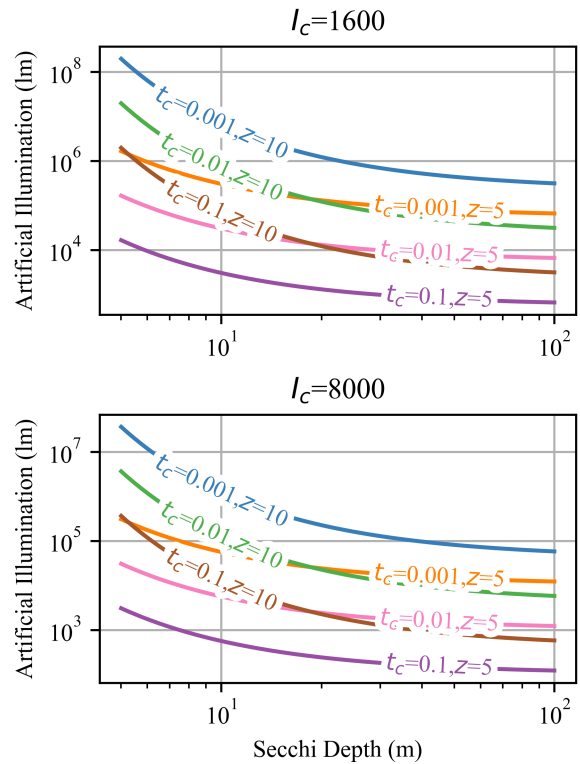


Figure 5. Example artificial illumination requirements to achieve certain exposures in various environments. $z_\Sigma = z_c = z$, $E_{v,A} = 0$, $r_S = 0.3$.

5. Model Validation

We have conducted some experiments to validate this model, and anticipate continuing to validate this model. Since it is difficult to precisely measure r_S and z_d , the majority of our tests will assess whether the model holds general trends and produces reasonable r_S and z_d . As this model is intended as a design estimation tool to predict lighting needs, it need not be exact.

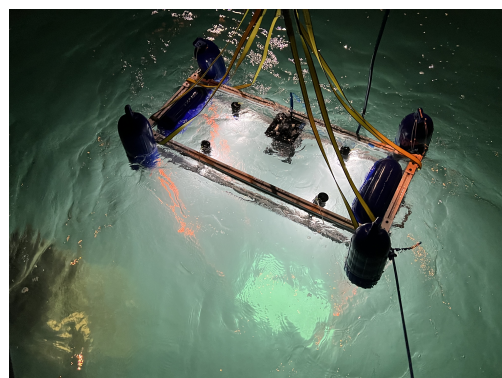


Figure 6. Lighting Test Rig deployed at UC San Diego's Ellen Browning Scripps Memorial Pier

This first major test was conducted on 2023-05-15 at the university's pier, shown in Figure 6. We attached a 20 MP machine vision camera⁴ and 40 000 lm of dive lights⁵ to a floating rig then placed a checkerboard target at various depths. At each

⁴ Lucid ATX204S with 8 mm lens

⁵ 4x BigBlue CB10000PBRC

depth stop, we executed several captures with varying exposures (0.143 ms to 51.2 ms) and gain values (4 dB to 32 dB). A subset of these data are shown in Figure 7.

Once we captured these data, we examined the exposure of each image, accepting only those whose peak pixel intensity was between 0.5 and 0.7 of full dynamic range. This results in the data shown in Figure 7.

We can visually estimate the Secchi distance at approximately 6 m - we cannot discern the edges of the checkerboard in the imagery at this depth. If we assume 30% reflectivity and an experimentally determined ISO/gain mapping of $I_c = 18 \times 10^{0.050g}$, then we get a very similar curve, as shown in Figure 7.

From the data, we see that we consistently get shorter exposure time at scene depths approaching the Secchi depth. This indicates that light reflecting from backscatter is impacting the scene exposure. If we fit the model to data collected up to 70% of the Secchi depth, we determine the best fit Secchi depth z_d to be 14 m and best fit scene reflectivity r_s to be 9%. The resulting curves and model differences are shown in Figure 8.

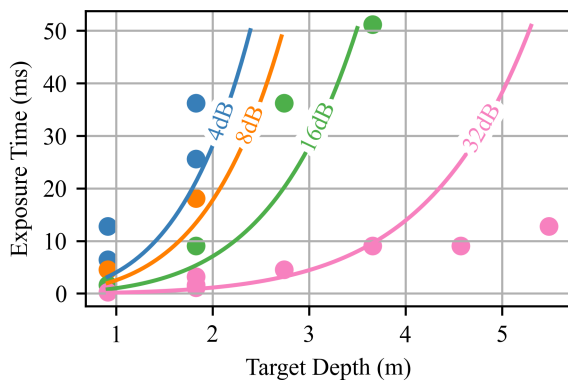


Figure 7. Accepted exposure values and predicted exposure values over depth from Lucid ATX204S

We conducted another set of tests on 2024-03-22 at the university's pier. For this experiment, we used a Nikon D780 with a 24 mm f/1.8 lens in a dive housing with 4 BigBlue 10 000 lm dive lights attached approximately 0.5 m on either side of the camera housing. We placed a checkerboard target at the base of the pier, then dove the camera in a vertical transect above the target while continuously capturing images. The camera was configured in aperture priority, ISO 8000. We measured the Secchi distance at approximately 2.8 m using a Secchi disk - this was also confirmed using the checkerboard. If we assume a 30% reflectivity, we get the curves shown in Figure 9.

In these data, we see that the model better fits the data. If we again fit the model to the data collected up to 70% of the Secchi depth, we determine the best fit Secchi depth z_d to be 14 m and the best fit scene reflectivity to be r_s to be 2.7%. The resulting curves and model differences are shown in Figure 10.

In both experiments we conducted, the model appears to overestimate the amount of light required to fully illuminate a scene, especially as the distance to scene approaches the Secchi depth (i.e. limit of visibility). Since this model does not account for light reflected due to backscatter, it falls apart when backscatter begins to dominate the reflectivity of the scene. Additionally, features in the scene will likely be indistinguishable when imaged close to the Secchi depth, which will likely cause the photogrammetric model to fail.

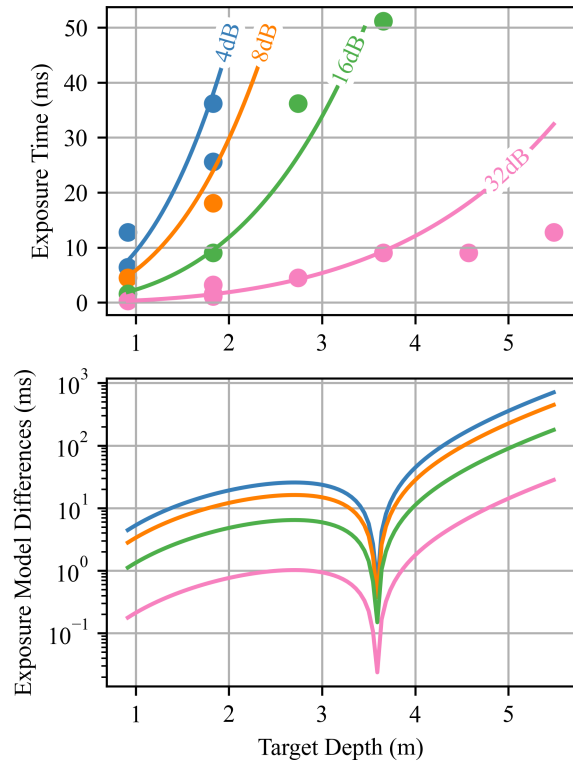


Figure 8. Accepted exposure values and best fit predicted exposure values over depth from Lucid ATX204S

6. Conclusion

In this paper, we propose and validate a mathematical model to estimate the amount of light required to achieve a well exposed image using only artificial illumination for underwater photogrammetry. This model is parameterized by Secchi depth, total artificial light, and camera exposure parameters. Experimental validation show that the model tends to imitate the exposure behavior in conditions where backscatter does not dominate the reflectance, and is otherwise off by less than 10 ms. This is likely enough to provide an engineering estimate to determine an appropriate amount of light.

Experimental validation indicates that this model begins to break down when imaging near the Secchi depth. The data suggests that more light is being reflected by the scene, which the model is not accounting for. In both experiments, the turbidity was due to fine particulates in the water column. In all likelihood, this model will also break down in the presence of large particulates in the water reflecting light. Additional work using different attenuation and reflectance turbidity models will assist this model in being more accurate in those regimes, however, such environments are not conducive to quality photogrammetry.

One particular application of interest is photogrammetric survey during times when ambient light is available. Availability of ambient light would affect the light entering the aperture of the camera, so modifications would be required to assess the contribution of ambient light. A reformulation of this model to allow arbitrary illumination sources, or to allow an additional arbitrary luminous source, would allow using the solar illuminance curves provided by Jones and Condit to estimate the maximum light required by a dive team (Jones and Condit, 1948).

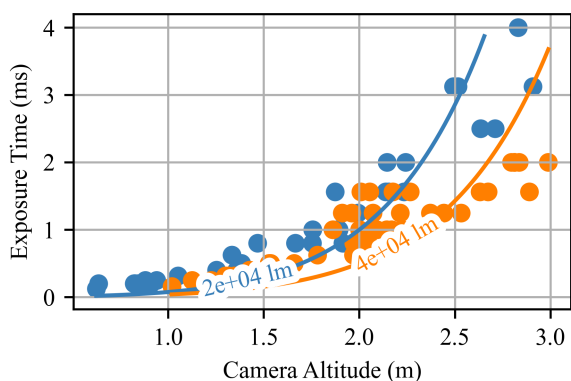


Figure 9. Exposure values and predicted exposure values over depth from Nikon D780

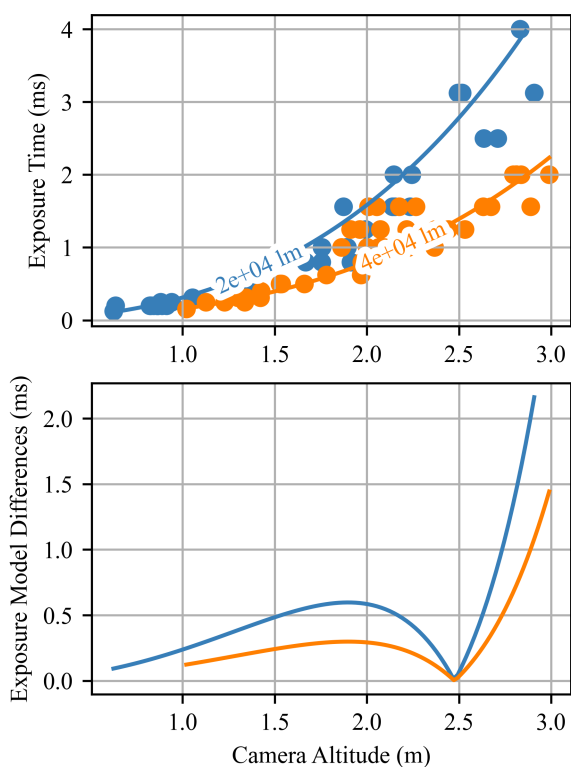


Figure 10. Exposure values and best fit predicted exposure values over depth from Nikon D780

7. Acknowledgements

This research was supported in part by the Office of Naval Research under award #N0001420C2023, Development of Scalable Multi-Sensor Coordination and Rapid Data Fusion Approaches for UUV Platforms, the USACE Engineer Research and Development Center Cooperative Agreement W9132T-22-2-0014, the National Science Foundation under award #CNS-1338192, MRI: Development of Advanced Visualization Instrumentation for the Collaborative Exploration of Big Data, and the Kinsella Expedition Fund. We also would like to thank the scientific divers at the Scripps Institution of Oceanography at UC San Diego, including Loren Clark, Jack Elstner, Analisa Freitas, Samantha Hanauer, Benjamin Klempay, and Christian McDonald, for supporting field experiments and operations, as well Brett Butler and the Prototyping Lab at Qualcomm Institute. Opinions, findings, and conclusions from this study are

those of the authors, and do not necessarily reflect the opinions of the research sponsors.

References

- Bobkowska, K., Burdziakowski, P., Szulwic, J., Zielinska-Dabkowska, K. M., 2021. Seven Different Lighting Conditions in Photogrammetric Studies of a 3D Urban Mock-Up. *Energies*, 14(23), 8002.
- Burdziakowski, P., Bobkowska, K., 2021. UAV Photogrammetry under Poor Lighting Conditions-Accuracy Considerations. *Sensors*, 21(10), 3531.
- Idso, S. B., Gilbert, R. G., 1974. On the Universality of the Poole and Atkins Secchi Disk-Light Extinction Equation. *The Journal of Applied Ecology*, 11(1), 399.
- International Organization for Standardization, 2019. Photography - Digital still cameras - Determination of exposure index, ISO speed ratings, standard output sensitivity, and recommended exposure index. <https://www.iso.org/standard/73758.html>.
- Jones, L. A., Condit, H. R., 1948. Sunlight and Skylight as Determinants of Photographic Exposure - Luminous Density as Determined by Solar Altitude and Atmospheric Conditions. *Journal of the Optical Society of America*, 38(2), 123–178. <https://opg.optica.org/abstract.cfm?URI=josa-38-2-123>.
- Song, B., Baik, D.-K., 2023. Illumination Processing Algorithm for Color Image Under Complex Illumination Conditions. *Journal of Computational and Theoretical Nanoscience*, 13(3), 2143-2156.
- Song, Y., Nakath, D., She, M., Köser, K., 2022. Optical Imaging and Image Restoration Techniques for Deep Ocean Mapping: A Comprehensive Survey. *PFG - Journal of Photogrammetry, Remote Sensing and Geoinformation Science*, 90(3), 243-267.
- Song, Y., Sticklus, J., Nakath, D., Wenzlaff, E., Koch, R., Köser, K., 2021. *Optimization of Multi-LED Setups for Underwater Robotic Vision Systems*. Springer International Publishing, 390–397.